Chapter 3

Observation of V-V Dimers Softening and Distinct Length Scales in Nanostructured VO_2 Thin Films

3.1 Introduction

A unit M_1-VO_2 cell (ρ_c = 4.66 g/cm3) contains z = 4 VO_2 ordered in "couples", so-called a 'dimer'. The VO_6^{8-} moieties spiral at the c-axis in uneven chains at 0.262 nm and 0.316 nm 'V^{4+}-V^{4+}' intervals along the a- and c-axes, respectively [1–3]. Molecular spectroscopy is widely used to probe VO_2 of its different polymorphs in terms of its phonons and photons [4–6]. An isolated VO_2 in an ideal gas has a ground state $2A_1$ (S = ½) according to its electron paramagnetic resonance (EPR) signal [7]. Assuming VO_2 is a molecule, two IR bands ν_1 = 946 cm^{-1} and ν_3 = 936 cm^{-1} is assigned as V-O symmetric and asymmetric stretching bands, respectively [8]. Nine phonon bands have been observed at the $2A_1$ state in a $VO_2 \rightarrow VO_2^-$ conversion [9]. Though phonon bands are well studied in characterizing different VO_2 polymorphs, no systematic study is made to assign the individual phonons in a VO_6^{8-} network [4, 8].

VO_2 has eighteen allowed phonon A_g and B_g modes in the low-temperature M_1 phase [10–12]. Marini et al. studied the effect of oxygen on the Raman spectra of VO_2 film and assigned the phonons at 195 cm^{-1} to a V-V vibration [13]. Lee et al. investigated Raman spectra of amorphous V_2O_5 [14]. They attributed phonons in the intermediate and high-energy region to different V-O vibrations [14]. At the same time, the phonons in the medium energy range can be associated with the different bending modes of V-O.

Structural properties of VO_2 through the SMT have been studied by Marezio et al. [15] and Atkin et al. [16] and others. Raman spectroscopy has utilized to investigate thin layers, micro and nano-beams and nanoparticles of VO_2 [14–18]. The knowledge of such phase transitions at the nano length-scale with high sensitivity to the polarization and symmetry is limited.

This chapter focuses on the study of a high-quality VO_2 thin film, fabricated on a SiO_2 coated (100) Si(p^{++}) substrates. Utilizing micro-Raman spectroscopy, we observe the formation and softening of V-V dimers across T_{SMT}. By recording current vs voltage (I-V) and resistance vs temperature (R-T) responses of VO_2 thin films, we measure the transport and electrical response of VO_2 thin films. An intriguing behaviour has observed for anti-stokes lines that are observed during a heating cycle of a VO_2 thin film across T_{SMT}. We provide direct evidence of V-V dimers softening and collapse that further restored which are in their initial phase after cooling. Our experimental findings suggest an abrupt optical switching at a lower temperature (T_o = 332 K), in contrast to a smooth resistive switching at a relatively higher temperature (T_c = 340 K). We argue that the notable difference in the transition temperatures (~ 8 K) attribute to the dependency of light scattering from the metallic domains, that are extended from the critical size needed for percolation conduction across SMT [19, 20]. A numerical simulation considering 2D-statistical nucleation and percolation model with mean-field approaches have performed to simulate the phase transitions. At the same time, the Mie scattering cross-section has utilized to explain the different scaling length scales observed in the optical and electrical transition temperature [19, 20].

3.2 Results and Discussion

3.2.1 Structural Analysis with XRD

XRD patterns were recorded to examine the phase purity of the VO_2 thin films. **Figure 3.1 (a & b)** shows the XRD pattern performed on the $VO_2/SiO_2(Si)$ sample. XRD pattern has a notable diffraction peak (011) at $2\theta = 27.29°$, with full width at half maximum (FWHM) of $w_{1/2} = 0.22°$, which is attributed to the monoclinic phase of VO_2. It is worth noting that the diffraction peak (011) position is slightly shifted compared to the theoretical value of 27.82°. This shift can be understood due to a lattice mismatch between the VO_2 film and the Si substrate, leading to a different value for interplanar distance, d = 3.26 Å. We estimated the average crystallite size (D_e) using Scherrer formula [21] as expressed in Eq. (1)

$$D_e = 0.9\,\lambda/(w.\cos\theta) \quad (1)$$

where *w* is FWHM of the diffraction peak that is estimated by interpolation at $2\theta = 27.29°$ using a pseudo-Voigt function (see **Figure 3.1 (b)**), λ is the wavelength, and θ is the diffraction angle corresponding to the peak (011) of VO_2. The value of $D_e = 38.47$ nm is estimated for the specimen $VO_2/SiO_2(Si)$ sample.

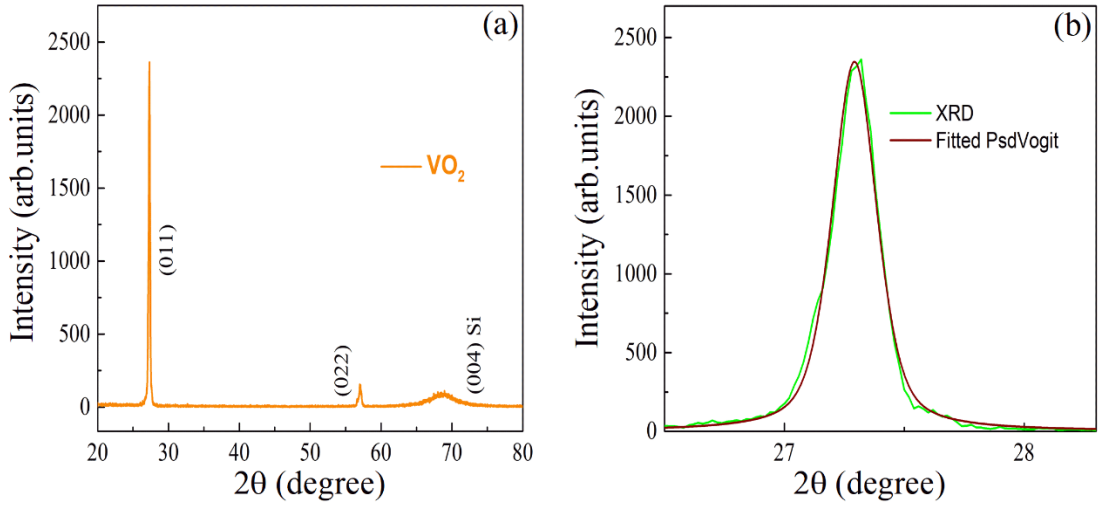

Figure 3.1 (a) The XRD spectra of VO_2 thin film. The Braggs peak across 27.29° and 57.11° correspond to the (011) and (022) peaks of the monoclinic (M_1) phase. (b) the highlighted part of (011) Bragg's peak along with its pseudo-Voigt function fit. Both experimental and simulation data are well-matched. An accurate value of the D_e is estimated.

3.2.2 TEM Characterization

Figure 3.2 (a & b) illustrates TEM images of a specimen VO_2 thin film. The average particle D_e is estimated to be ~110 nm. TEM image indicates VO_2 thin films grow in form of particles of variable shapes and sizes. The particles will grow in the form of the isolated islands above the critical thickness. A high-resolution TEM image of a such particle reveals the (011) orientation corresponding to the d-spacing of 3.14 Å that matches with the monoclinic phase of VO_2. Above the critical thickness, the strain relaxes and VO_2 nucleates discretely. **Figure 3.2 (a & b)** shows the state of art observation of such a growth mechanism. The results indicate that the grain size distribution in the sol-gel derived VO_2 film is mediated by the density of the nucleation centre that can vary with different extents of thermal deformation during the annealing. The crystallite coalescence will further increase the thickness. The lattice extends along a preferred direction during

a balancing act between the surface energy and free energy of the grain boundaries (011). **Figure 3.2 (a & b)** shows the high-resolution TEM image acquired from the tip of the NCs. High-resolution TEM images of VO_2 crystallites reveal the lattice fringes, indicating high degree of crystallinity [21–23].

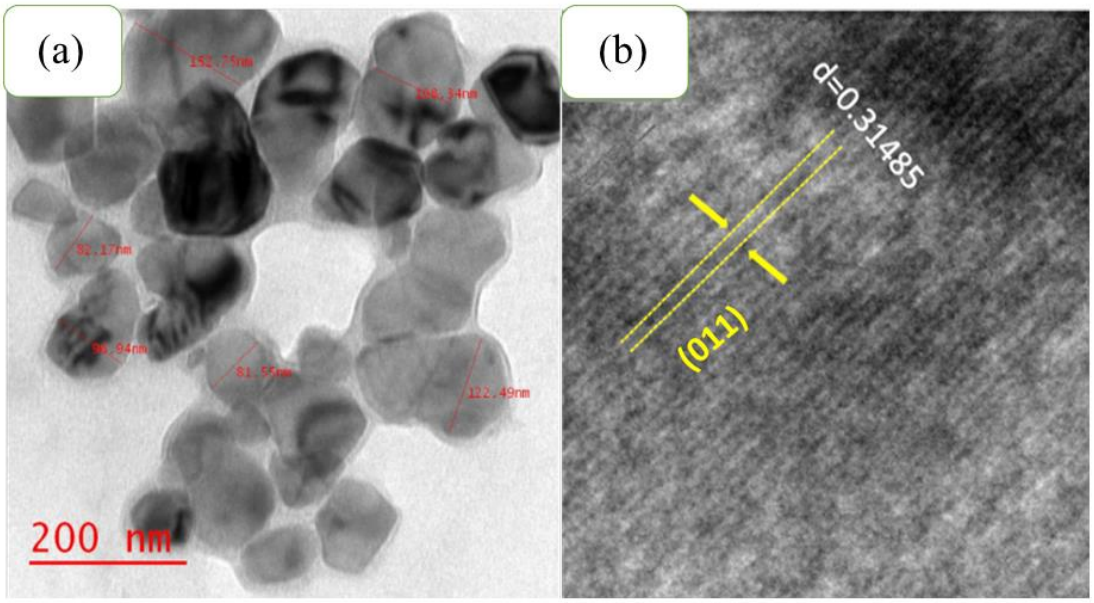

Figure 3.2 VO_2 NCs were imaged through a TEM at a nano-length scale by dispersing crystallites on top of a carbon-coated mesh. (d) Illustrates the well-ordered lattice fringes in (011) crystallographic direction, imaged by employing HR-TEM.

3.2.3 I-V Characteristics and Temperature Dependence of Sheet Resistance

Figure 3.3 (a) shows I-V characteristics measured in vertical geometry from 0 to 5 V at RT. Voltage-triggered SMT is observed at RT with V_{th} at 1.28 V. The width of the voltage triggered SMT window is ~ 1 V. Considering the 54 nm thickness of the VO_2 thin film, the threshold electric field for initiating SMT is approximately order of 107 V/m at RT,

which is in good agreement with studies on both VO_2 planar junctions on sapphire and capacitor-type devices on silicon [24–27]. Similar characteristics were also observed for VO_2 planar junctions by Sharoni et al. [28]. Electric field-induced SMT has revived by conducting AFM in regions more petite than a single grain size to get staircase free steps in the I-V curves [26–28]. **Figure 3.3 (b)** shows the PF plot log(I/V) vs √V of the I-V curves. At large voltages 2.25 V, the VO_2 thin film shows metallic behaviour over a broad temperature range. At voltage = 1.19 V, the VO_2 shows mixed-phase behaviour and acts as an SC at a lower temperature.

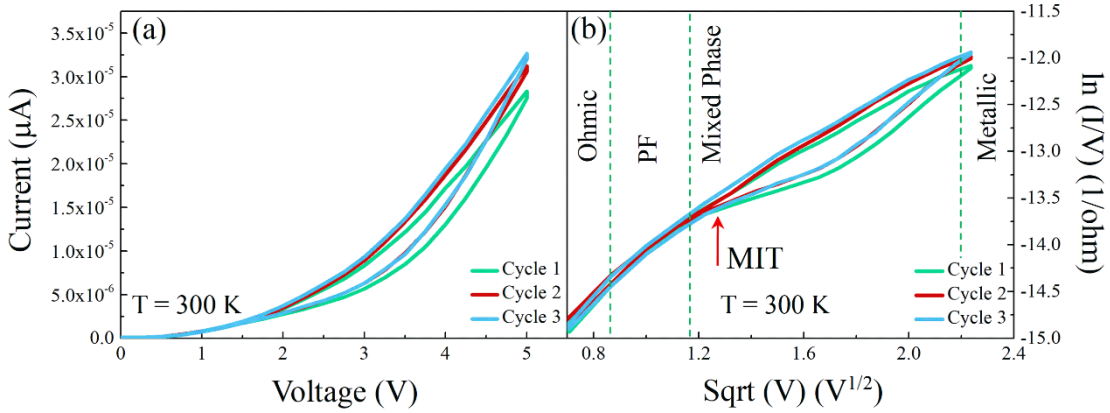

Figure 3.3 (a) I-V characteristics of the $VO_2/SiO_2(Si)$ measured in vertical geometry between 0-5 V at RT. The electric-field-triggered SMT is observed at RT. (b) PF plot of the I-V curves log(I/V) vs √V. Three regions metallic, Ohmic and PF dominating are defined. The dotted green lines in the PF region are for visual guidance, indicating the dominating of the PF conduction mechanism in that region.

At intermediate bias voltages and below thermal SMT, the PF mechanism dominates the conduction as indicated by the linear dependence of log(I/V) over √V [29]. The dotted lines in **Figure 3.3 (b)** are used for visualizing the different dominating conduction mechanisms. Four areas, namely: Ohmic, PF, mixed and metallic are denoted that suggest the dominant conduction mechanism in each region. These results indicate that either at

high-temperature (or larger applied voltages), the VO_2 enters a pure metallic state due to the thermally or electrically triggered SMT [29]. Whereas below SMT, at lower temperatures and small bias voltages, Ohmic behaviour is predominant in VO_2. At low temperature and intermediate bias voltage, the PF mechanism dominates. Defects, such as oxygen vacancies in VO_2, may serve as localized traps required for PF conduction. Before the onset of the metallic state, the localized states assist the PF conduction under electric field bias [28, 29].

3.2.4 Temperature Dependent Raman Spectroscopy

Figure 3.4 (a & b) shows Raman spectra acquired at multiple temperatures across SMT during heating-cooling cycles from the nanostructured VO_2 thin films under investigation. The complete spectra contain several peaks that match Raman bands assigned to monoclinic VO_2 [15–18]. The peaks near 192.1 and 222.5 cm^{-1} correspond to characteristic A_g symmetry vibrational modes of the low-temperature monoclinic structure of VO_2 that diminish upon transition into the high-temperature tetragonal phase. These phonon modes play a significant role in the structural transition of VO_2, since they are control the pairing and tilting motions of V-V dimers, which map the monoclinic phase onto the tetragonal lattice configuration [15–18]. Raman bands are located at RT at frequencies 192.1 and 222.5 cm^{-1} are associated an additional feature at 188.6 and 206.1 cm^{-1}. Raman peaks intensities diminish in the heating cycle as the phase transition is approached.

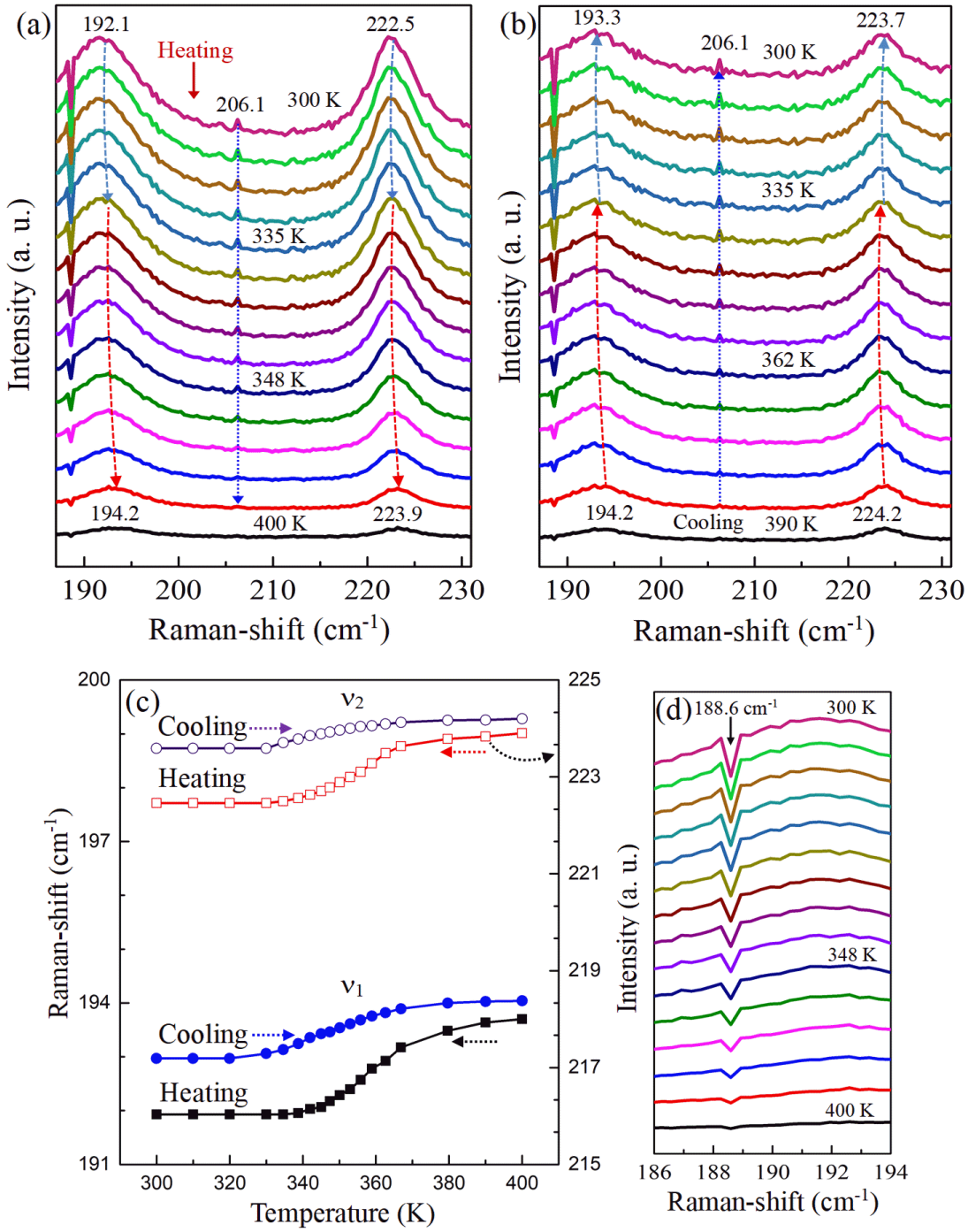

Figure 3.4 Raman modes measured for representative VO_2 thin film as a function of temperature during (a) Heating and (b) cooling cycles. The Raman frequencies ν_1 and ν_2 show the FWHM and intensity vary as a function of temperature, suggesting a robust structural link, (c) variation of Raman frequencies ν_1 and ν_2 during heating/cooling cycles, (d) evidence of hole burning in Raman spectra during a heating and cooling cycle.

The complete disappearance of the 192.1 cm^{-1} peak at sufficiently high temperatures suggests that VO_2 thin film does not contain trackable fraction of the V_2O_5 phase, the ultimate oxidation state of vanadium. These Raman bands reappear again during cooling process (**Figure 3.4 (b)**). The disappearance of the Raman peaks was used to estimate T_0 (332 K) in NCs of VO_2 thin film [14–17].

A good agreement is found between the temperatures at which the Raman features become weak across T_{SMT}, which is well-matched from T_{SMT} measured through temperature dependence of resistance across SMT (**Figure 3.5**). The observed Raman lines at 192.1 and 222.5 cm^{-1} represent the V-V and V-O related Raman bands. **Figure 3.4 (d)** highlights the additional feature obtained at frequencies 188.6 cm^{-1}, known as hole burning. A phase diagram (T vs FWHM) is constructed to distinguishes the semiconducting, mixed and metallic regions. The intermediate region is attributed to a mixed-phase, as depicted in **Figure 3.4 (b & c)**. The phase diagram summarizes changes in the width of V-V (ν_1) and V-O (ν_2) modes versus temperature in the heating/cooling cycles [15–17]. **Figure 3.4 (c)** shows the dependence on Raman ν_1 and ν_2 frequencies during heating/cooling cycles. Temperature-dependent Raman lines at ν_1 and ν_2 frequencies confirm a blue shift across SMT during heating/cooling cycles. For considered sample a blue shift is noticed for frequency ν_1 between 300 and 370 K, above which a steady blue shift emerges. A similar overall dependence is seen for frequency ν_2, with an initial blue shift temperature across SMT followed by a constant blue shift at higher temperature ($T > T_{SMT}$) [14–18]. This correlation confirms a gradual phase transformation in the VO_2 and suggests that the blue shift is related to the rising carrier

concentration. For VO_2, a simple phase diagram is expected, in which the material is a narrow-gap SC below T_{SMT} and conductor above this temperature [10–12].

3.2.5 Numerical Simulation of Nucleation and Percolation Process During Phase Transition

Figure 3.5 (a) illustrates T onset and T_{SMT} values of resistance as a function of temperature for nanostructured VO_2 thin film. A good correlation between temperature dependencies of the resistance and Raman data is expected to confirm the existence of semiconducting, mixed and metallic regions as designated in the phase diagram as illustrated in **Figure 3.5 (b & c)**. **Figure 3.5 (a)** suggests that the mixed-phase extends over 340-360 K. However, **Figure 3.5 (b & c)** confirms that the mixed-phase ranges from 330-365 K. For VO_2 thin films, the shape, sharpness, position, width and switching of the thermal hysteresis have reported to depend on the quality of the VO_2 thin films such as stoichiometry, crystallinity, impurities, the grain size and their distribution and orientation [10].

To understand this contradictory observation, we employed the 2D-Bruggeman effective medium approximation that allowed us to estimate the change in resistance in terms of the metallic phase fractions and charge puddles size. Mie scattering simulation was also performed to access more optical properties that depict a link between the changes in scattering cross-section for a percolative media [19, 20]. **Figure 3.5 (d)** summarizes the results obtained by simulation that estimate the variation in macroscopic resistance curves during a heating/cooling cycle as a function of metallic charge puddles size, which is dispersed in a homogeneous semiconducting matrix in a non-interacting manner [19, 20]. At metallic phase fraction of 0.5, scattering occurs at T = 320 K [19, 20], where the sheet resistance is approximately 3.0 and 3.5 KΩ during heating and cooling cycles,

respectively. We noted that relative to the change in resistance, the scattering cross-section is shifted in temperature across the hysteresis, with a larger hysteresis width [19, 20]. A change in the semiconducting fraction appears to induce a difference in resistance.

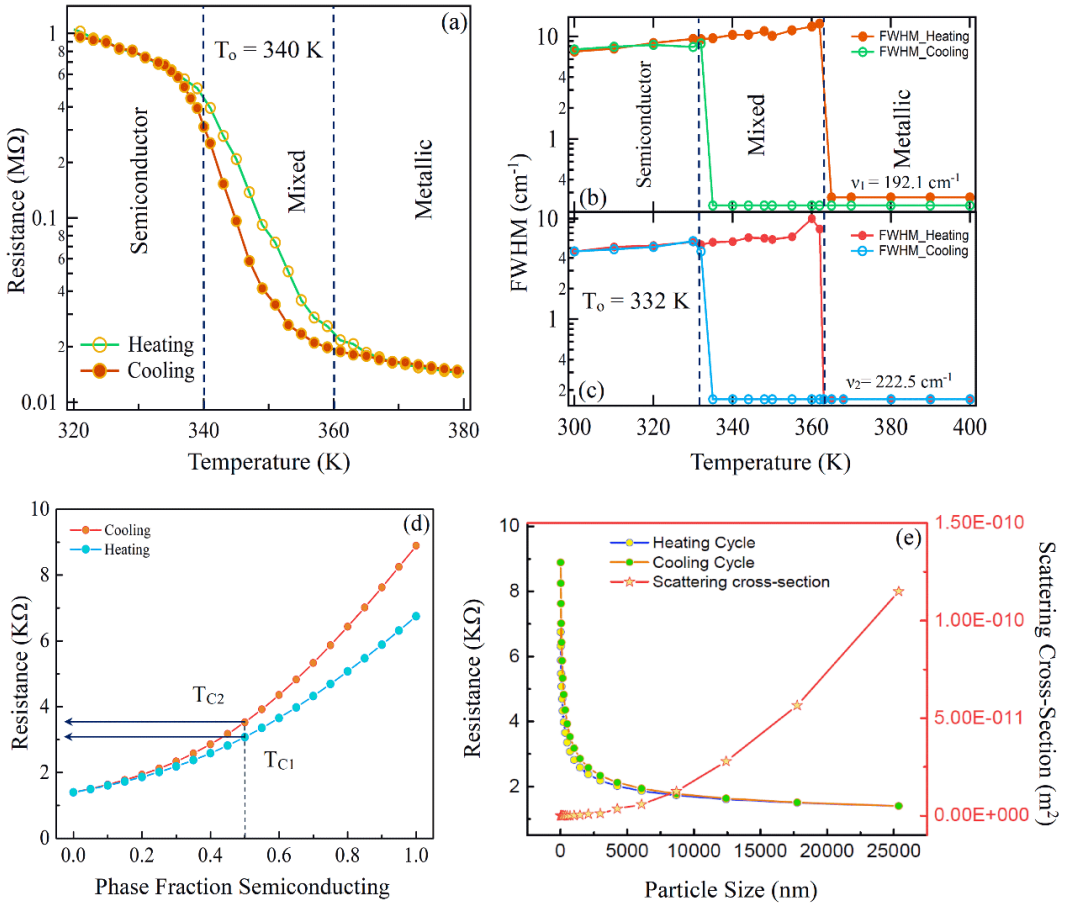

Figure 3.5 (a) The temperature-dependent sheet resistance of representative VO_2 thin film. The change in resistance suggests three different regions: SC, mixed-phase and metallic phase. (b) The variation of FWHM of V-V dimers (b) (191.93 cm$^{-1)}$ and (c) V-O bond (222.5 cm^{-1}) frequencies as a function of temperature across the SMT during heating/cooling cycles. (d) Resistance vs puddles size plot, which is simulated for both heating and cooling. For each thermal cycle, critical temperatures, T_{C1} and T_{C2}, are shown. Dashed vertical lines indicate T_{C1} and T_{C2} calculated from EMA during heating/cooling cycles. (e) The scattering cross section as a function of puddles size is well corroborated with resistance vs puddles size plot.

The change in optical scattering cross-section is deviated during heating and cooling cycles (**Figure 3.5 (d)**). One can justify the above claims by defining a critical phase

fraction/puddle (particle) size that describes T_c for heating/cooling cycles. The explanation of shift in scattering discussed in the previous paragraphs is that the decrease in IR scattering cross-section is due to Mie scattering by charge puddles evolving during the Mott transition [19]. A variation in resistance requires the metallic puddles to have a high enough density to generate a continuous conducting route at a higher temperature [21, 30].

We note that the metallic charge puddles are on the length scale of 0.50 μm at RT. While the scattering cross-section is kept changing in the cooling cycle even over temperatures, the metallic puddles are expected to be 0.5-1.0 μm. These findings reconfirm the assumption that the scattering changes, although no conducting route exists [30, 31]. During the transition of VO_2, a mixed-phase is evolved only within a narrow range of transition temperatures for both heating/cooling cycles [31–33]. Since mixed-phase represents spatial inhomogeneity, it is equally essential to explore their scattering behaviour to explain the significant temperature shifts optical transitions. We simulated mixed-phase optical constants that require stabilizing nanoscale charge puddles during the transition [31–33].

3.3 Conclusion

In conclusion, we investigate the temperature induced phase transition in a nanostructured VO_2 thin film of M_1 phase with wide variations in sample morphology using thermal, Raman spectroscopy and I-V curve measurements. The experimental findings suggest that lowering the energy barrier between M_1 and R phases promote the growth of spatially inhomogeneous phases. The optical phase transition proceeds as described by Raman spectroscopy, with a transition from M_1 through some intermediate phase to R with a characteristic time scale. Despite the variations in sample morphology, the simulated

dependences indicate that variable sizes for charge puddles size between the phases are universally present in VO_2 samples. Thus, the metallic phase and optical switching that exploits this phase transition may be limited to switching behaviours independent of VO_2 morphology. Spatially inhomogeneous mixed-phase presence is manifested, which causes modulation in scattering cross-section that further explains the significant temperature shifts during optical transitions.

REFRENCES

[1] J. Lin, H. Ji, M. W. Swift, W. J. Hardy, Z. Peng, X. Fan, A. H. Nevidomskyy, J. M. Tour, and D. Natelson, "Hydrogen Diffusion and Stabilization in Single-Crystal VO_2 Micro/Nanobeams by Direct Atomic Hydrogenation," *Nano Letters*, **14** (2014) 5445–5451.

[2] W. R. Mondal, E. Evlyukhin, S. A. Howard, G. J. Paez, H. Paik, D. G. Schlom, L. F. J. Piper, and W. C. Lee, "Role of V-V Dimers on Structural, Electronic, Magnetic, and Vibrational Properties of VO_2 by First-Principles Simulations and Raman Spectroscopic Analysis," *Physical Review B*, **103** (2021) 214107–214113.

[3] X-Ray Powder Diffraction JCPDS files, (a) 01-082-661; VO2 Monoclinic, (b) 01-079-1655; VO_2 rutile, and (c) Si-P63mc, Joint Committee on Powder Diffraction Standard International Centre for Diffraction Data, Swarthmore, PA, USA, 2019.

[4] M. Zaghrioui, J. Sakai, N. H. Azhan, K. Su, and K. Okimura, "Polarized Raman Scattering of Large Crystalline Domains in VO_2 Films on Sapphire," *Vibrational Spectroscopy*, **80** (2015) 79–85.

[5] S. Lee, T. L. Meyer, C. Sohn, D. Lee, J. Nichols, D. Lee, S. S. A. Seo, J. W. Freeland, T. W. Noh, and H. N. Lee, "Electronic Structure and the Insulating Gap in Epitaxial VO_2 Polymorphs," *APL Materials*, **3** (2015) 126109 (7).

[6] S. Singh, T. A. Abtew, G. Horrocks, C. Kilcoyne, P. M. Marley, A. A. Stabile, S. Banerjee, P. Zhang, and G. Sambandamurthy, "Selective Electrochemical Reactivity of Rutile VO_2 Towards the Suppression of Metal-Insulator Transition," *Physical Review B*, **93** (2016) 125132–125138.

[7] L. B. Knight, R. Babb, M. Ray, T. J. Banisaukas, L. Russon, R. S. Dailey, and E. R. Davidson, "An Electron Spin Resonance Investigation of Vanadium Dioxide ($^{51}V^{16}O_2$ and $^{51}V^{17}O_2$) and $^{51}V^{17}O$ in Neon Matrices with Preliminary Assignments for VO_3 and V^{+2}: Comparison with Ab-Initio Theoretical Calculations," *Journal of Chemical Physics*, **105** (1996) 10237–10250.

[8] Y. Gong, M. Zhou, and L. Andrews, "Spectroscopic and Theoretical Studies of Transition Metal Oxides and Dioxygen Complexes," *Chemical Reviews*, **109** (2009) 6765–6808.

[9] J. B. Kim, M. L. Weichman, and D. M. Neumark, "High-Resolution Anion Photoelectron Spectra of TiO_2^-, ZrO_2^-, and HfO_2^- Obtained by Slow Electron Velocity-Map Imaging," *Physical Chemistry Chemical Physics*, **15** (2013) 20973–20981.

[10] G. I. Petrov, V. V. Yakovlev, and J. Squier, "Raman Microscopy Analysis of Phase Transformation Mechanisms in Vanadium Dioxide," *Applied Physics Letters*, **81** (2002) 1023–1025.

[11] E. U. Donev, R. Lopez, L. C. Feldman, and R. F. Haglund Jr., "Confocal Raman Microscopy across the Metal-Insulator Transition of Single Vanadium Dioxide Nanoparticles," *Nano Letters*, **9** (2009) 702–706.

[12] R. Srivastava, and L. L. Chase, "Raman Spectrum of Semiconducting and Metallic VO_2," *Physical Review Letters*, **27** (1971) 727–730.

[13] C. Marini, E. Arcangeletti, D. D. Castro, L. Baldassare, A. Perucchi, S. Lupi, L. Malavasi, L. Boeri, E. Pomjakushina, K. Conder, and P. Postorino, "Optical Properties of $V_{1-x}Cr_xO_2$ Compounds under High Pressure," *Physical Review B*, **77** (2008) 235111 (9).

[14] S. H. Lee, H. M. Cheong, M. J. Seong, P. Liu, C. E. Tracy, A. Mascarenhas, J. R. Pitts, and S. K. Deb, "Microstructure Study of Amorphous Vanadium Oxide Thin Films Using Raman Spectroscopy," *Journal of Applied Physics*, **92** (2002) 1893–1897.

[15] D. B. McWhan, M. Marezio, J. P. Remeika, and P. D. Dernier, "X-Ray Diffraction Study of Metallic VO_2," *Physical Review B*, **10** (1974) 490–495.

[16] J. M. Atkin, S. Berweger, E. K. Chavez, M. B. Raschke, J. Cao, W. Fan, and J. Wu, "Strain and Temperature Dependence of the Insulating Phases of VO_2 Near the Metal Insulator Transition," *Physical Review B*, **85** (2012) 020101 (4).

[17] Y. Gu, J. Cao, J. Wu, and L. Q. Chen, "Thermodynamics of Strained Vanadium Dioxide Single Crystals," *Journal of Applied Physics*, **108** (2010) 083517 (7).

[18] J. Cao, Y. Gu, W. Fan, L. Q. Chen, D. F. Ogletree, K. Chen, N. Tamura, M. Kunz, C. Barrett, J. Seidel, and J. Wu, "Extended Mapping and Exploration of The Vanadium Dioxide Stress-Temperature Phase Diagram," *Nano Letters*, **10** (2010) 2667–2673.

[19] E. Arcangeletti, L. Baldassarre, D. D. Castro, S. Lupi, L. Malavasi, C. Marini, A. Perucchi, and P. Postorino, "Evidence of a Pressure-Induced Metallization Process in Monoclinic VO_2," *Physical Review Letters*, **98** (2007) 196406 (4).

[20] H. R. Seren, G. R. Keiser, L. Cao, J. Zhang, A. C. Strikwerda, K. Fan, G. D Metcalfe, M. Wraback, X. Zhang, and R. D. Averitt, "Optically Modulated Multiband Terahertz Perfect Absorber," *Advanced Optical Materials*, **2** (2014) 30–33.

[21] D. Li, W. Huang, L. Song, and Q. Shi, "Thermal Stability of VO_2 Thin Films Deposited by Sol-Gel Method," *Journal of Sol-Gel Science and Technology*, **75** (2015) 189–197.

[22] Y. Zhao, J. H. Lee, Y. Zhu, M. Nazari, C. Chen, H. Wang, A. Bernussi, M. Holtz, and Z. Fan, "Structural, Electrical, and Terahertz Transmission Properties of VO_2 Thin Films Grown on C-, R-, and M-Plane Sapphire Substrates," *Journal of Applied Physics*, **111** (2012) 053533 (8).

[23] P. Shvets, O. Dikaya, K. Maksimova, and A. Goikhman, "A Review of Raman Spectroscopy of Vanadium Oxides," *Journal of Raman Spectroscopy*, **50** (2019) 1226–1244.

[24] A. L. Patterson, "The Scherrer Formula for X-Ray Particle Size Determination," *Physical Review*, **56** (1939) 978–982.

[25] N. F. Quackenbush, H. Paik, M. J. Wahila, S. Sallis, M. E. Holtz, X. Huang, A. Ganose, B. J. Morgan, D. O. Scanlon, Y. Gu, F. Xue, L. Q. Chen, G. E. Sterbinsky, C. Schlueter, T. L. Lee, J. C. Woicik, J. H. Guo, J. D. Brock, D. A. Muller, D. A. Arena, D. G. Schlom,

and L. F. J. Piper, "Stability of the M2 Phase of Vanadium Dioxide Induced by Coherent Epitaxial Strain," *Physical Review B*, **94** (2016) 085105 (6).

[26] H. Qiu, M. Yang, Y. Dong, H. Xu, B. Hong, Y. Gu, Y. Yang, C. Zou, Z. Luo, and C. Gao, "The Tetragonal-Like to Rutile Structural Phase Transition in Epitaxial VO_2/TiO_2 (001) Thick Films," *New Journal of Physics*, **17** (2015) 113016 (8).

[27] A. Frenzel, M. M. Qazilbash, M. Brehm, B. G. Chae, B. J. Kim, H. T. Kim, A. V. Balatsky, F. Keilmann, and D. N. Basov, "Inhomogeneous Electronic State Near the Insulator-to-Metal Transition in the Correlated Oxide VO_2," *Physical Review B*, **80** (2009) 115115 (7).

[28] A. Sharoni, J. G. Ramírez, and I. K. Schuller, "Multiple Avalanches Across the Metalinsulator Transition of Vanadium Oxide Nanoscaled Junctions," *Physical Review Letters*, **101** (2008) 026404 (4).

[29] J. Kim, C. Ko, A. Frenzel, S. Ramanathan, and J. E. Hoffman, "Nanoscale Imaging and Control of Resistance Switching in VO_2 at Room Temperature," *Applied Physics Letters*, **96** (2010) 213106 (3).

[30] P. P. Boriskov, A. A. Velichko, A. L. Pergament, G. B. Stefanovich, and D. G. Stefanovich, "The Effect of Electric Field on Metal-Insulator Phase Transition in Vanadium Dioxide," *Technical Physics Letters*, **28** (2002) 406–408.

[31] Z. Yang, C. Ko, and S. Ramanathan, "Metal-Insulator Transition Characteristics of VO_2 Thin Films Grown on Ge (100) Single Crystals," *Journal of Applied Physics*, **108** (2010) 073708 (6).

[32] S. Kirkpatrick, "Percolation and Conduction," *Reviews of Modern Physics*, **45** (1973) 574–588.

[33] A. S. Alexandrov, A. M. Bratkovsky, and V. V. Kabanov, "Phase Coexistence and Resistivity Near the Ferromagnetic Transition of Manganites," *Physical Review Letters*, **96** (2006) 117003 (4).